# Crater formation by single ions in the electronic stopping regime: Comparison of molecular dynamics simulations with experiments on organic films

E. M. Bringa* and R. E. Johnson
*Engineering Physics, University of Virginia, Charlottesville, Virginia 22903*

R. M. Papaléo
*Faculdade de Física, Universidade Católica do Rio Grande do Sul, CP 1429, Porto Alegre, RS, Brazil*
(Received 16 May 2001; revised manuscript received 22 August 2001; published 20 February 2002)

An incident fast ion in the electronic stopping regime produces a track of excitations which can lead to particle ejection and cratering. Molecular dynamics simulations of the evolution of the deposited energy were used to study the resulting crater morphology as a function of the excitation density in a cylindrical track for large angles of incidence with respect to the surface normal. Surprisingly, the overall behavior is shown to be similar to that seen in the experimental data for crater formation in polymers. However, the simulations give greater insight into the cratering process. The threshold for crater formation occurs when the excitation density approaches the cohesive energy density, and a crater rim is formed at about six times that energy density. The crater length scales roughly as the square root of the electronic stopping power, and the crater width and depth seem to saturate for the largest energy densities considered here. The number of ejected particles, the sputtering yield, is shown to be much smaller than simple estimates based on crater size unless the full crater morphology is considered. Therefore, crater size cannot easily be used to estimate the sputtering yield.

DOI: 10.1103/PhysRevB.65.094113 PACS number(s): 61.80.Jh, 79.20.Ap, 34.50.Fa

## I. INTRODUCTION

Surface modification of materials by single-ion irradiation has been studied in insulators,[1–6] semiconductors,[7–9] and metals[10,11] using electron, scanning tunneling (STM), and atomic force (AFM) microscopes. A large variety of features have been observed: ''bumps,''[9] craters,[1–5,12–14] crater rims (hillocks),[1–5,15,16] adatoms,[8,17] and surface roughening.[18] Cratering occurs in response to the pressure pulse and fluid flow to the surface produced by the rapid deposition of energy, but the process is not understood quantitatively. ''Bumps'' generally appear when an energetic process occurs a few layers below the surface, creating a low-density region with a larger volume which raises the surface.[19] When the energy loss per unit path length of the projectile, $dE/dx$, and the sputtering yield are relatively small, adatoms are observed in both experiments and simulations. By increasing the energy deposition (and the yield) craters are eventually formed. For very large energy deposition and yields, redeposition of the ejecta plus plastic deformation occurs, producing craters with rims, studied recently for ion bombardment of polymers[5] and other organic materials.[1,3]

Craters are also produced by cluster ion bombardment which can lead to huge sputtering yields.[20,21] This process has been studied in the velocity regime in which nuclear (elastic) energy loss dominates over electronic energy loss and has been seen in both, experiments[20,22] and simulations.[23–26] The simulations are generally performed for bombardment at normal incidence and when energy is deposited in momentum transfer collisions to the target atoms. There are few simulations of cratering in the electronic regime[27] and none for non-normal incidence.

At normal incidence the crater produced by a fast incident ion has a roughly circular profile, but recent experiments have focused on ions incident at a large angle with respect to the normal[2–5] and at grazing incidence.[13] Even at normal incidence molecular dynamics (MD) results for keV ion clusters incident on a copper surface appear to disagree with the scaling laws followed by macroscopic cratering[14] in which the crater radius varies with the bombarding energy[28] $E$ as $E^{1/3}$. For oblique incidence in polymers[5] and biomolecules[3] bombarded by fast heavy ions it was found that the crater width does not increase significantly with increasing deposited energy density, whereas the size of the crater along the incident ion direction increases rapidly with increasing energy density.

In this paper MD simulations are used to study the surface morphology produced by the energy deposited by fast ions incident at large angle with respect to the surface normal. The results of these simulations are compared to models for the length, width, and depth of the crater versus the energy density (i.e., $dE/dx$ and track width). Since crater formation is used for sculpting specific surface features for biomolecule adsorption[29], for determining surface properties,[4] and for estimating sputtering yields,[5,3] we use MD simulations to extract scaling laws for crater formation. Although the simulations are for an ''atomic'' solid, quite remarkably, the trends are very similar to those recently seen in polymers.[5]

## II. MD SIMULATION

Following the passage of a fast heavy ion a cylindrically energized region is produced in a solid, which we refer to as a track of excitations. A Lennard-Jones (LJ) crystalline solid is simulated with particles interacting through the potential[30] $V(r)=4\varepsilon[(r/\sigma)^{-6}-(r/\sigma)^{-12}]$. Although this is an oversimplified model of a real solid, this two-parameter potential has the advantage that the equations of motion, and hence, all results including the crater dimensions, scale with $\varepsilon$ and $\sigma$. In addition, certain weakly bound solids, such as the low-

 

temperature, condensed-gas solids, can be reasonably approximated as LJ solids, with parameters $\varepsilon$ and $\sigma$ taken to reproduce the material properties. All LJ samples have a cohesive energy $U \approx 8\varepsilon$. The interlayer distance for (001) layers is $d \approx 0.78\sigma$ and the bulk modulus is $B = 75\varepsilon/\sigma^3$. More details on the MD simulation can be found elsewhere.[30–32] As in our earlier papers, the scaling with $\varepsilon$ and $\sigma$ is replaced by scaling using $U$ and the number density $n$. For the fast processes which determine sputtering and cratering, we showed that the scaling was roughly preserved when a more complex potential was used.[33]

Since the results will be compared to data on polymers, we note that certain polymers are roughly simulated using a LJ potential for the interchain interactions, plus a stronger potential to account for the covalent interaction within the chain.[34] A typical size for $\sigma$ in polymers is 3.5–5 Å.[34] The cohesive energy of a polymer is more difficult to define. The covalent bonds among atoms in the same polymer chain are of the order of several eV's with slightly weaker bonds between monomers in a chain. However, the bonding among atoms in the neighboring chains is very weak, much smaller than 1 eV, making the binding field ''anisotropic.'' Removing a small chain requires different energies depending on the chain orientation and entanglement. The average cohesive energy is usually taken to be equal to the sublimation energy. A simple estimate[35] gives $U \approx 0.5$ eV/monomer. Therefore, even though the LJ calculations scale with size and binding energy, we assume an effective binding energy of 0.5 eV/particle and $\sigma = 5$ Å so that our ''atoms'' very crudely represent monomers. The melting temperature for this solid is $T_m \approx 500$ K. This is close to the tabulated value for ''crystalline'' PMMA, $T_m \sim 460$ K,[36] and to the value of $T_m$ (523 K) used by Szenes *et al.*[37] for polyethylene teraphtalat (PET). The mass of the simulated particle, $M$, only changes the time scale, which is given by the dimensionless time $t/t_0$, where $t_0 = \sigma\sqrt{M/\varepsilon}$. Assuming a mass of $70u$ gives $t_0 = 1.75$ ps.

The stopping power, i.e., the energy deposited per unit length $dE/dx$, and the effective track radius, here $r_{cyl}$, are typically used to describe the energy density deposited by the ion in its passage through the solid. Since in the electronic sputtering regime only a fraction of the experimental $dE/dx$ goes into nonradiative deexcitations, in the following we use the symbol $(dE/dx)_{eff}$ to represent the amount of energy deposition contributing to track formation, cratering, and sputtering. The amount of deposited electronic energy that actually goes into energetic atomic motion and the radial scale of that energy is not well known at present either in a polymer or in a condensed gas solid. Estimates of this fraction in insulators are within 0.1–0.4.[37–39] Here, as a guidance, we use the value 0.2, as estimated from experiments in polymers[37] and condensed gas solids.[39] The remaining 80% of the deposited energy is dispersed to phonons at larger distances from the track, trapped electrons, etc., with typically a small fraction lost radiatively as discussed elsewhere.[40,41]

Thermal spike models have been applied recently to estimate the latent track radius in irradiated polymers with positive results.[37] To mimic the nonradiative energy release at the ion track in the MD simulations all $N_{exc}$ particles within a cylinder of radius $r_{cyl}$ are given an energy $E_{exc}$ with their velocities in random directions, where $N_{exc}$ is the number of excitations per layer parallel to the initial surface. Therefore, $(dE/dx)_{eff}$ is $N_{exc}E_{exc}/d$.

The radius of the ultratrack,[40] given as the maximum range of the $\delta$ electrons, has been used as the track radius in some studies. However, for sputtering and surface modification, the spike radius $r_{cyl}$ is often associated with the radius of the infratrack, which can be estimated from $r_B$, the Bohr adiabatic radius.[40–42] Since $r_B$ does not vary significantly in the energy range of the experiments by Papaléo *et al.*,[5] all simulations were run for an initial track radius $r_{cyl} = 2\sigma = 10$ Å, which is of the same order of magnitude as $r_B$. We have recently examined the assumption that $r_{cyl} \approx r_B$,[39] but a fixed $r_{cyl}$ of 1 nm is a reasonable assumption based on the physics of the tracks. In this paper a radius of 1 nm implies $N_{exc} \approx 10/\cos\Theta$. The incident angle $\Theta$ is measured in degrees with respect to the surface normal. For all simulations $\Theta = 60°$. Larger angles were not feasible as the sample size required became too large to practically simulate. Therefore, the stopping power from MD is multiplied by a factor $\cos 60°/\cos 79°$ to compare to experiments done at $\Theta = 79°$.

The overall size of the sample in each simulation, from $3\times10^4$ up to $2.5\times10^5$ particles, was estimated for a given $E_{exc}$ such that the final temperature of the sample was well below melting. After each calculation we checked that the thickness of the sample was large enough that there were unperturbed layers below the crater. We also checked that the crater borders were far away from the lateral boundaries. Our MD code can apply a number of boundary conditions (BC's),[30,31] and we verified that different BC's did not change the crater size. For several cases we ran the simulation with a sample of twice the size and verified that the results did not change within the standard error. The total simulation time was also increased with $E_{exc}$ from $20t_0$ up to $40t_0$, to be able to ''detect'' all ejected particles and allow the crater walls to cool down below the melting temperature. Most quantities presented are averages of results from a number of simulations (4–20) in which the directions of the energized atoms were randomly varied.

## III. CRATER FEATURES

A cut across a crater formed following an excitation event is shown in Fig. 1. This cut is in a plane containing the initial surface normal and the track direction and shows the maximum depth of the crater. The crater wall is seen to have a slope similar to the incident ion direction on the entrance side and a very steep slope at the back. Remarkably, this shape is very stable even in this model solid as we have increased the run time by a factor of 2 and see little relaxation occurring. This is the case because of the rapid cooling in the track core discussed elsewhere.[31,43] At the end of a typical simulation ($\sim 30t_0$) the temperature is $\sim 50$ K higher than the initial temperature of the sample (30 K), far from the melting temperature of the model solid. Of course, over very long times, relaxation can occur in an atomic material even at relatively low temperatures, whereas it is less likely in a glassy polymer. Therefore, crater morphology in polymers can be readily studied. Despite some problems

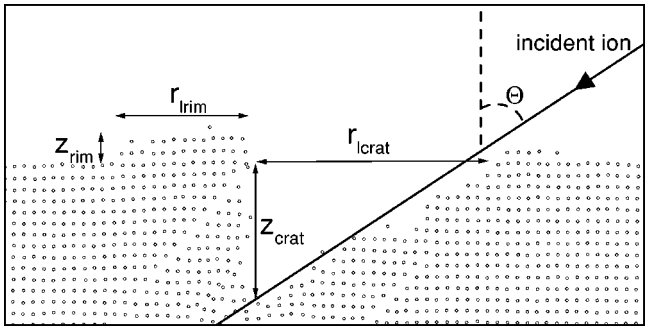


FIG. 1. Slice of the final configuration of one MD cratering event, showing a side view of the crater and crater rim. The incident ion impact angle is $\Theta = 60°$ and $(dE/dx)_{eff} \approx 330U/\sigma = 330$ eV/nm. The different dimensions of the defect are shown in the figure.

with their interpretation, scanning force microscopy measurements[16] are regularly used to analyze heavy ion damage in solids.

Since all craters were found to have a characteristic morphology, the dimensions used in the subsequent graphs and discussions are indicated in Fig. 1. This crater is formed at high excitation densities (12.5 *nU*) and exhibits a rim on the back side. Not all craters, however, have rims, as we will discuss. To ''see'' the rim better, in Fig. 2 we show a top view of a crater,[44] together with an AFM image of a 20 MeV Au impacting on a PMMA film. The rim is primarily on the sides and the back of the crater, not at the ion entrance site. This is the case even when there is no momentum preferentially deposited along the incident angle as is the case in macroscopic cratering. Here the crater is formed from a cylindrical ''heat spike'' but has many of the characteristics associated with impact cratering. We also note that atoms on the rim borders are aligned along the preferential ⟨110⟩ directions, indicating recrystallization of the material pushed or deposited onto the surface. For this ''atomic'' material a few adatoms are also seen far from the track region.

The crater formation has several stages, but most of the crater volume is ejected before $\sim 20t_0$ (35 ps for a mass of $70u$). Temperature varies greatly during the formation process and near the center of the track it can be larger than the melting temperature even after $10t_0$. The dependence of the crater dimensions on the energy deposited in the track can be seen in Fig. 3. The experimental data of Papaléo *et al.*[5] for 5–197 MeV $Au^+$ bombardment of PMMA are also shown. The MD values represent the mean value of the crater dimension for 4–20 simulations at each $(dE/dx)_{eff}$. Each MD simulation gives a slightly different sized crater. The size distribution is narrow and becomes narrower with increasing crater size. The maximum difference between the mean value of the size and values for individual simulations was used to obtain the error bars shown in the figures. Experimentally, for a fixed projectile and irradiation condition, the morphology of the craters on PMMA and many other organic films so far tested[1–5,16] varies only slightly for different impacts. Craters are usually elliptical and elongated in the direction of ion penetration, with a dispersion in size of roughly 20%. The crater rims may vary a bit more in shape. In some cases the rims are seen around the crater as in Fig. 2; in others the rims are seen only as a tail behind the craters. Also the contours of the rims are irregular, though similar in overall size.

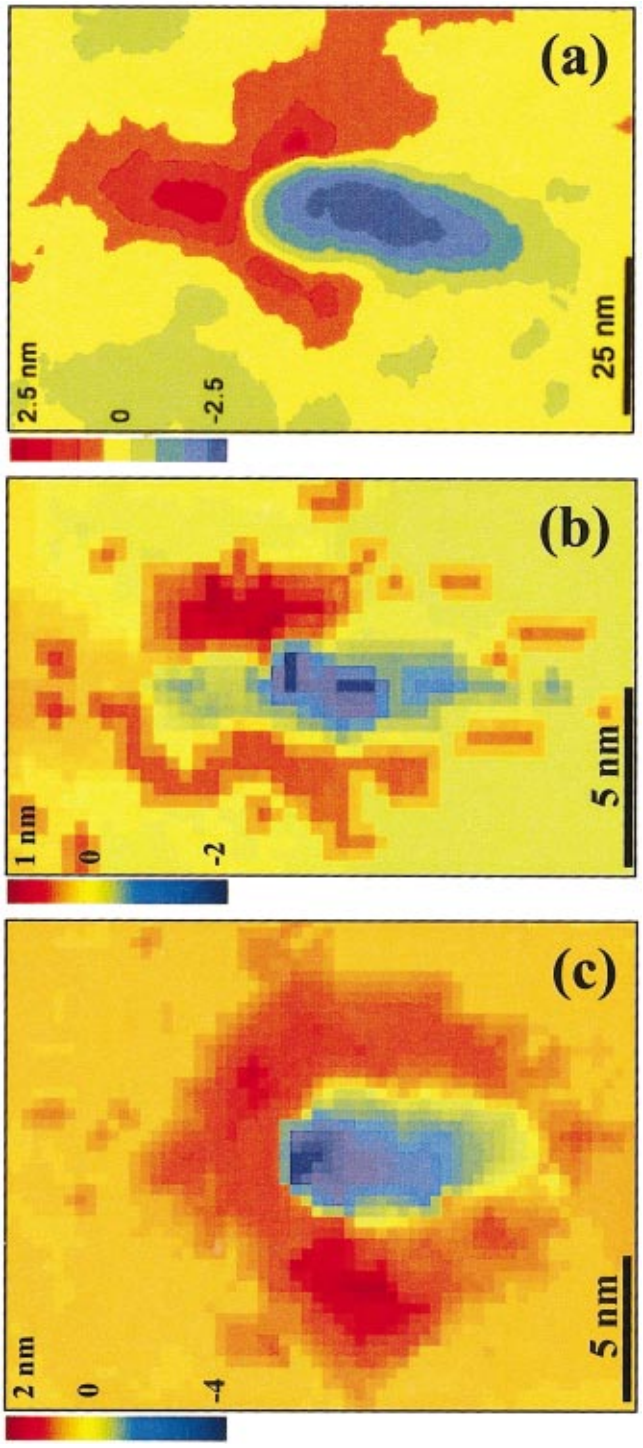


FIG. 2. (Color) Top view of a crater, where the color scale indicates height. (a) Experimental result for $\Theta = 79°$ and $(dE/dx)_{eff} = 660$ eV/nm (20 MeV Au on PMMA). (b) MD simulation for $\Theta = 75°$ and $(dE/dx)_{eff} = 205$ eV/nm. (c) MD simulation for $\Theta = 60°$ and $(dE/dx)_{eff} = 330$ eV/nm. Because of differences in $\Theta$ and energy, the MD crater in (c) is not as elongated as the experimental crater.

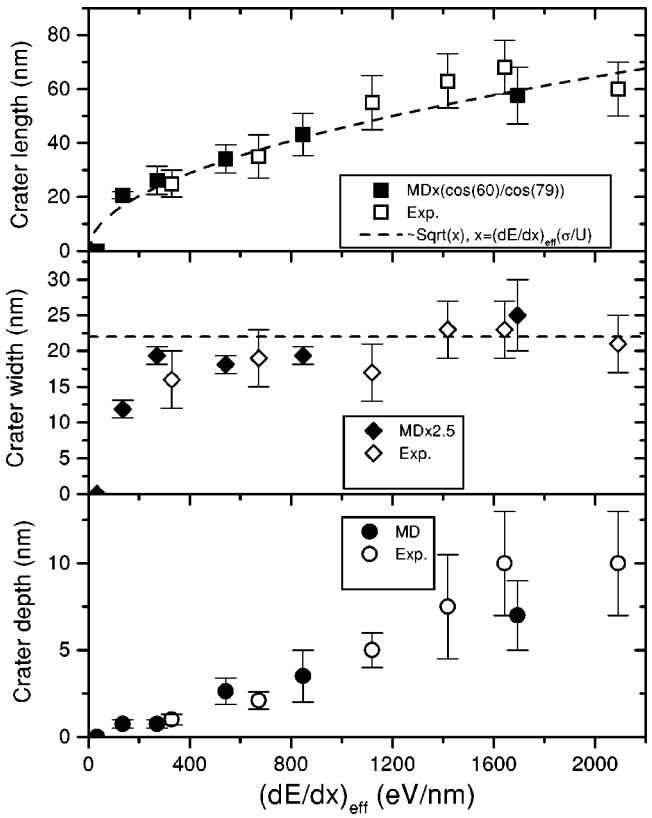


FIG. 3. Crater size as a function of $(dE/dx)_{eff}$. MD results for $\Theta = 60°$, $U = 0.5$ eV, $\sigma = 5$ Å, and taking $(dE/dx)_{eff} = 0.2(dE/dx)$. MD crater length is multiplied by a factor $(\cos 60°/\cos 79°)$ to account for the different incident angle in the simulation. Open symbols are experimental data from Papaléo *et al.* (Ref. 5).

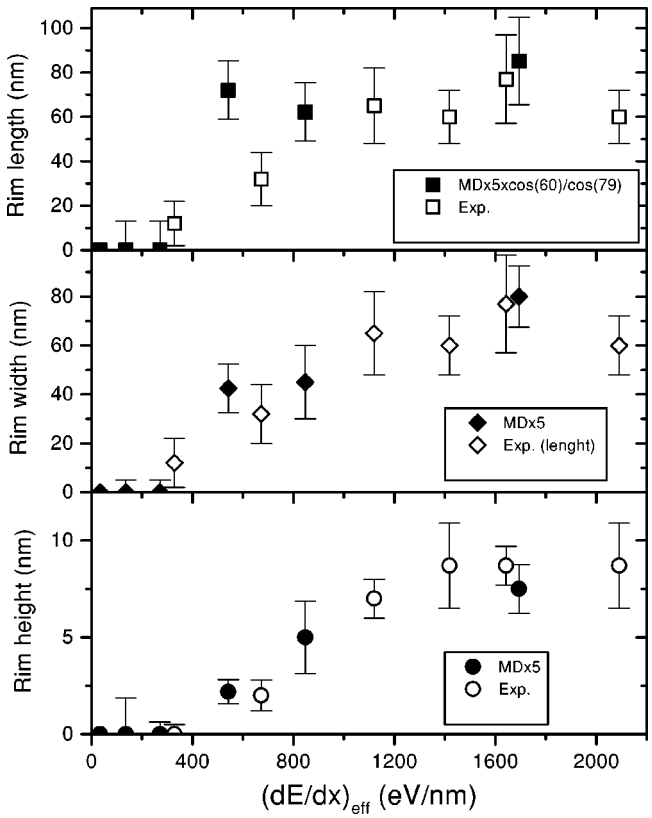


FIG. 4. Same as Fig. 3, but showing rim size as a function of $(dE/dx)_{eff}$. MD sizes are multiplied by 5 in order to compare trends with the experiment.

Because of sample size limitations, angles above 60° are problematic whereas experimental results are often performed at nearly grazing incidence. In previous work,[32] the width of the distribution of original position of the ejecta along the direction of the incident beam was found to have a $\cos^{-1}\Theta$ dependence while no variation was found in the distribution along the perpendicular direction. Therefore, in order to compare the simulations with the experiments a $\cos^{-1}\Theta$ dependence has been assumed for lengths along the direction of incidence of the ion. Some preliminary results from simulations and experiments for tracks at different angles (including $\Theta = 75°$) support this assumption. As mentioned before, the MD results for crater and rim length obtained at $\Theta = 60°$ were multiplied by a factor $\cos 60°/\cos 79°$ when comparing to the data of Papaléo *et al.*[5]

Exact quantitative agreement is not expected for the crater dimensions because of our simplified model solid. Moreover, experimental results are the convolution of the actual crater profile with the AFM tip shape and may also involve some late relaxation of the crater walls. Therefore, the measured depth is expected to be smaller than the actual depth, but the effect of the convolution is smaller for the other crater dimensions. For all these reasons the MD results were normalized separately for the length, width, and depth comparisons in Fig. 3. However, it is seen, quite remarkably, that the trends in the experiment and in the simulation are the same. This indicates that useful scaling laws can be obtained and that the crater formation process is insensitive to the details of both the energy deposition profile and the materials properties. This also means that simulations for relatively simple systems can be used to predict crater structures when using ions to modify materials. Using a different value (instead of 0.2) for the fraction of the stopping power going into material deformation and sputtering would only shift the points in Figs. 3–5 without any influence in the scaling.

For the shock model of Yamamura and co-workers[45,46] given in the Appendix, the volume of ejecta is determined by the energy density deposited, and the crater length and width are *both* expected to increase as $\sqrt{(dE/dx)_{eff}}$. Assuming that the volume removed and the crater size are directly related, this gives a $(dE/dx)_{eff}^{3/2}$ dependence for the sputtering yield. The crater length is seen in Fig. 3 to increase roughly as $\sqrt{(dE/dx)_{eff}}$ in both the simulations and the experiments. However, the length appears to increase more slowly and to saturate at large values of $(dE/dx)_{eff}$. After a steep increase, the crater width is seen to be much smaller than the length and increases only very slowly with increasing $(dE/dx)_{eff}$. The crater depth is much smaller than both the length and the width but appears to increase with $(dE/dx)_{eff}$. The pressure pulse model, also discussed in the Appendix, gives such a scaling, but it also predicts that all of the dimensions have the same scaling. That model gave a good fit to MD calculations of the *sputtering yield* for ejec-

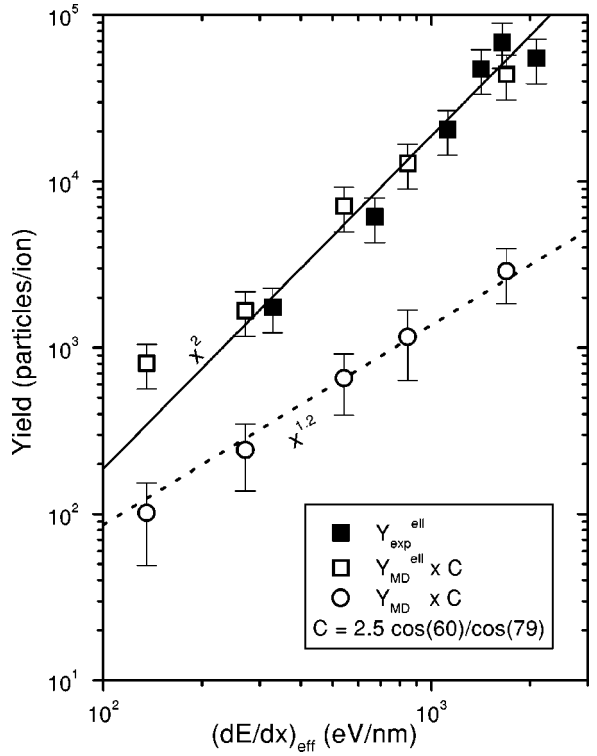


FIG. 5. Sputtering yield as a function of $(dE/dx)_{eff}$. Yields obtained assuming the crater is an ellipsoid: $Y_{expt}^{ell}$ from experiments of ion bombardment of polymers (Ref. 5) (solid squares), $Y_{MD}^{ell}$ from the size of MD craters in Fig. 3 (open squares). The ''true'' MD yields $Y_{MD}$ are also shown (open circles). Lines are only a guide to the eye.

tion of large LJ molecules with hard cores, at normal incidence, and appeared to agree with data from a solid made of large biomolecules.[27] However, its predictions differ from what is seen in the simulations presented here and in the experiments with polymers[5] and the amino acid valine.[2]

Although it is not clear from Fig. 3, for $E_{exc}$ below $U$ (i.e., the energy density in the track is less than the cohesive energy density) no crater is formed for the $r_{cyl}$ used here. A threshold is also seen in the experiments and, therefore, crater detection can give a measure of the cohesive energy. Below the threshold, several atoms escape from the top layers, leaving vacancies, and the sputtering yield is small, as discussed by Bringa *et al.*[31] In addition, some atoms are displaced to the top layer, where they stay as adatoms, but an identifiable crater is not observed. For $6U > E_{exc} > 2U$ a shallow crater forms for these track parameters and again several atoms are relocated as adatoms on the surface. For $E_{exc} > 6U$ the energy density is close to the bulk modulus of the material, slip dislocations appear, and a crater rim is formed. The dimensions of the rim are shown in Fig. 4 as a function of $(dE/dx)_{eff}$. After the initial rise at ''threshold'' the rim length and width stay constant within our error bars, but the rim height increases very slowly with $(dE/dx)_{eff}$. Again, these trends are also observed experimentally, which is quite remarkable considering the differences in materials.

## IV. SPUTTERING YIELD

The sputtering yield can, of course, be obtained directly from the MD simulations. We showed earlier the surprising result that at the high excitation densities for which the energized track produces craters, the sputtering yield $Y_{MD}$, is not predicted by standard models. $Y_{MD}$ is roughly proportional to $(dE/dx)_{eff}$ times the effective ''sputter depth,'' which is a fraction of the initial track width.[31,32] When it is difficult to measure directly, the sputtering yield is often approximated by an estimate of the crater volume. This has been tested for normal incidence for LJ molecules with a core.[27] Here we evaluate that procedure for large incident angle for a standard LJ solid. Typically one assumes that the ejected volume is a semiellipsoid, $Y^{ell} = (\pi/6) n r_{cl} r_{cw} z_c$, where $r_{cl}$, $r_{cw}$, and $z_c$ are the crater length, width, and depth, respectively. This rough estimate is based on crater shapes obtained from MD and has been used in several papers.[5] In Fig. 5 we show $Y^{ell}$ for the polymers[5] ($Y_{expt}^{ell}$) obtained as in Papaléo *et al.*[5] using a semiellipsoidal volume and the same number density as in the MD simulations (using $M = 70u$ gives a density of 0.98 g/cm$^3$). We also show the estimate based on the MD crater ($Y_{MD}^{ell}$) using the values in Fig. 3. These are both compared to the actual MD yield $Y_{MD}$ as a function of $(dE/dx)_{eff}$, where the MD yields have been multiplied by $C = 2.5 \cos(60°)/\cos(79°)$, which results from the normalization in Fig. 3.

The estimated ''yield'' for the polymer is seen to be larger than that estimated from the MD craters, but, remarkably, the trends are the same. They both give a yield that depends roughly quadratically on $(dE/dx)_{eff}$. This is, fortuitously, the same dependence predicted by thermal spike models for sputtering,[47] which has lead to misinterpretation of the physics of ejection. However, it is seen that these yield estimates are an order of magnitude larger than $Y_{MD}$ and that they have a steeper dependence on $(dE/dx)_{eff}$. Therefore, such methods for estimating the sputtering yield are unreliable. This large discrepancy is due to several factors. First, the craters are not well approximated by a half ellipsoid. Second, for the excitation energies shown many of the atoms originally in the crater relocate on the rim. Third, there are regions of higher density at the crater walls. These factors add up to a surprisingly large overestimate of the experimental yield. More importantly, since the ratio $Y_{MD}^{ell}/Y_{MD}$ changes with $(dE/dx)_{eff}$, the dependence of the yield with $(dE/dx)_{eff}$ cannot be obtained from such estimates. Since most of the atoms on the rim come from the crater region, a more detailed description of the morphology of the crater needs to be made to obtain a reasonable yield estimate.

## V. DISCUSSION AND SUMMARY

Here we carried out a series of MD simulations to study crater formation due to the high energy density deposited in a cylindrical ''track.'' Such an energized track might be formed by a penetrating fast ion that deposits its energy in electronic excitations, which is of interest here, or deposits its energy by momentum transfer, producing recoil atoms. That is, the craters described are not impact craters like the

lunar craters;[28] rather, they are the craters formed in response to the rapid energy deposition in the track of an energetic ion. The study here is for large angles of the track with respect to the surface normal and we studied the dependence on the cohesive energy of the material and on the energy density deposited by an incident ion.

First, we showed that the crater structure remains stable in this Lennard-Jones material over the longest simulations time tested ($\sim 75t_0$), which is much larger than the crater formation time ($\sim 20t_0$). This is the case because of the rapid cooling of the track by the melting and pressure pulse processes described in earlier papers.[31,43] We also found the initially surprising result that the scaling of the crater parameters with $(dE/dx)_{eff}$ in this LJ solid agrees remarkably well with that found experimentally for MeV heavy ion bombardment of polymers at 79° to the normal.[5] This means that concepts learned from MD simulations of simple materials can be applied to more complex materials.

As shown earlier for the experimental data for polymers,[5] we find a threshold for crater formation and a second threshold for rim formation. In another set of experiments the rims could be removed when the polymer is maintained at higher temperatures, so that viscous relaxation occurs. Therefore, Papaléo *et al.*[4] used the relaxation of rim formation versus material temperature to locate the glass transition temperature. Here we did not vary the material temperature as late relaxation occurring over long time periods cannot be described using MD. However, in this paper we are able to relate the two thresholds to the track energy density. Our MD simulations show that the threshold for crater formation occurs when the energy density in the track is close to the cohesive energy density or, in the track formation model used here, when the nonradiative relaxation energy per particle inside the initial track, $E_{exc}$, is near the sublimation energy $U$. The threshold for rim formation, however, occurs at a higher energy density both in the experiment and in the simulations. We find this to be $E_{exc} \approx 6U$ for the relevant track widths. This occurs when the energy density in the track roughly equals the bulk modulus of the material. In the crystalline material slip dislocations can form at such energy densities, allowing the raised structure to be maintained. Using an efficiency of[37] 0.2 for converting electronic excitation energy into energetic lattice motion and the estimated $r_{cyl}$, we find that the experimental value of the stopping power needed to form a rim in a polymer would be around 2 keV/nm for $\Theta = 79°$, consistent with the measured value.[5]

Above the threshold the crater width is found to be nearly constant for large incident angles and the crater length and depth increase sublinearly with $(dE/dx)_{eff}$. The rim height is 10 times smaller than its length and grows faster than the crater size (depth and length). This dependence should be compared to the steeper dependence for the crater radius and depth at normal incidence.[12]

We note that for nonpenetrating cluster bombardment the crater scaling with energy deposited is different from that found here. For incident clusters the energy of the projectile is deposited close to the surface. For a projectile energy $E$, the crater volume $V$ is found to follow[48] $V \propto (E/U)$. However, recent MD simulations seem to indicate that for keV copper clusters on copper scaling is[14] $V \propto (E/U^2)$. It was argued that the presence of a molten region in the MD simulation caused the steeper dependence on $U$. New MD results from simulations of keV xenon ions on gold[49] support the quadratic dependence with $U$ and relate this to the formation of a melt. It is difficult to compare these results with ours in which the energy is deposited in a long cylindrical track. Assuming that the energy relevant for crater formation is deposited in a volume close to the surface of depth $L$, $E = (dE/dx)_{eff} L$, we find $V \propto (E/U)^2$. Here we also find that the molten region is important in the crater formation. Clustering of the ejecta might also affect crater size[12], but in our simulations, unlike the embedded atom model (EAM) Cu used in several cluster bombardment simulations,[14] there is almost no contribution of clusters to the sputtering yield.

Finally, we examined the practice of estimating the sputtering yield by parametrizing the crater volume. Recent results by Insepov *et al.*[48] point to a possible connection between crater size and hardness, and claim that crater volume is also related to the sputtering yield. However, they find a different dependence on the bombarding energy for the yield ($Y \propto E^{1.4}$) and for the crater size ($V \propto E$), confirming the discrepancy found here [$Y \propto (dE/dx)_{eff}^{1.2}$ and $V \propto (dE/dx)_{eff}^{2}$]. We showed that, for the model material studied here, using crater size to estimate sputtering yield can produce surprisingly large errors in the sputtering yield and, even, the wrong dependence on $(dE/dx)_{eff}$. Therefore, if the yield cannot be measured directly, the full morphology of the crater and rim needs to be described to get an accurate yield. Although the detailed nature of the ejecta (clusters, angular distribution, and so on) depends on the details of the interaction potential used, the total sputtering yield seems to be insensitive to the potential.[50]

## ACKNOWLEDGMENTS

This work was supported by the National Science Foundation Astronomy and Chemistry Divisions. We are grateful for useful comments from H. M. Urbassek, K. H. Nordlund, Z. Insepov, and E. Hall.

## APPENDIX A: SHOCK MODELS FOR SPUTTERING AND CRATER FORMATION

There are several related models which attempt to explain sputtering at high excitation density using shock waves. Also, the collision of an impactor with a target producing spallation has been extensively studied with MD,[51] together with cluster bombardment-induced shock waves.[25,52] The spallation process originates from the interaction of two rarefaction waves, one coming from the shock wave reflected at the surface and the other coming from the impactor.[53] Yamamura and co-workers[45,46] estimated the sputtering yield due to shock waves with spherical symmetry intersecting a surface. They suggested that a hemispherical volume is ejected with radius $r_c$. Then the yield $Y$ is proportional to the volume of the ejecta ($\sim 2\pi r_c^3/3$) with $r_c \sim (dE/dx)_{eff}^{1/2}$. Bitensky and Parilis[54] considered cylindrical tracks and the incident angle dependence to model biomolecule sputtering. At

normal incidence their model reduced to the spherical shock model. The crater dimensions are assumed to be proportional to $\sqrt{(dE/dx)_{eff}}$.

In order to explain experiments on ejection of whole biomolecules[27] where $Y \propto (dE/dx)_{eff}^3$, Fenyö and Johnson[27] proposed the pressure pulse (PP) model. In the PP model, there are many excitation events along the ion track, each contributing to $(dE/dx)_{eff}$ as in the simulations described here. Whereas the energy density evolves diffusively, the net energy density gradient causes a net volume force and, therefore, a net momentum transfer radially and towards the surface. If the net momentum transfer to a certain volume is larger than some critical momentum, that volume will be ejected. This determines a critical radius $r_c \propto (dE/dx)_{eff}$, with the volume ejected proportional to $r_c^3$. The PP model predicts an angular distribution peaked at 45° and agrees well with MD simulations that use a Lennard-Jones potential with a core to describe the interactions of large excited molecules.[27] Notice that the PP model gives crater dimensions proportional to $(dE/dx)_{eff}$. If a critical energy for ejection is considered,[55] instead of a critical momentum, the yield is $Y \propto (dE/dx)_{eff}^{3/2}$, as in Kitazoe *et al.*[45]

In all models discussed above the width and length of the crater have the same dependence on $(dE/dx)_{eff}$. When oblique ion incidence is considered the yield increases as $1/\cos\Theta$ because the length of the crater increases also as[12] $1/\cos\Theta$. Therefore, the $(dE/dx)_{eff}$ dependence is the same as at normal incidence, which is not what is found in the simulations presented here.

*Present address: Lawrence Livermore National Laboratory, Materials Science and Technology Division, Chemistry and Materials Science Directorate, P.O. Box 808, L-353 Livermore, CA 94551. Electronic address: bringa1@llnl.gov

[1] J. Kopniczky, C. T. Reimann, A. Hallén, B. U. R. Sundqvist, P. Tengvall, and R. Erlandsson, Phys. Rev. B **49**, 625 (1994).
[2] J. Eriksson, J. Kopniczky, G. Brinkmalm, R. M. Papaléo, P. Demirev, B. U. R. Sundqvist, P. Håkansson, and C. T. Reimann, Nucl. Instrum. Methods Phys. Res. B **101**, 142 (1995).
[3] J. Eriksson, J. Rottler, C. T. Reimann, and B. U. R. Sundqvist, Int. J. Mass Spectrom. Ion Processes **175**, 293 (1998).
[4] R.M. Papaléo, L. D. de Oliveira, L. S. Farenzena, M. A. de Araújo, and R. P. Livi, Phys. Rev. B **62**, 11 273 (2000).
[5] R. M. Papaléo, L. S. Farenzena, M. A. de Araújo, R. P. Livi, M. Alurralde, and G. Bermudez, Nucl. Instrum. Methods Phys. Res. B **148**, 126 (1999).
[6] F. Thibaudau, J. Cousty, E. Balanzat, and S. Bouffard, Phys. Rev. Lett. **67**, 1582 (1991).
[7] K. Kyuno, D. G. Cahill, R. S. Averback, J. Tarus, and K. Nordlund, Phys. Rev. Lett. **83**, 4788 (1999).
[8] K. Nordlund, M. Ghaly, R. S. Averback, M. Caturla, T. Diaz de la Rubia, and J. Tarus, Phys. Rev. B **57**, 7556 (1998).
[9] Q. Yang, T. Li, B. V. King, and R. J. MacDonald, Phys. Rev. B **53**, 3032 (1996).
[10] H. Dammak, A. Dunlop, D. Lesueur, A. Brunelle, S. Della-Negra, and Y. Le Beyec, Phys. Rev. Lett. **74**, 1135 (1995).
[11] R. C. Bircher and S. E. Donnely, Nucl. Instrum. Methods Phys. Res. B **148**, 194 (1999).
[12] C. T. Reimann, Nucl. Instrum. Methods Phys. Res. B **95**, 181 (1994).
[13] I. V. Vrobyova, Nucl. Instrum. Methods Phys. Res. B **146**, 379 (1998).
[14] R. Aderjan and H. M. Urbassek, Nucl. Instrum. Methods Phys. Res. B **163-64**, 697 (2000).
[15] A. Müller, C. Müller, R. Neumann, and F. Ohnesorge, Nucl. Instrum. Methods Phys. Res. B **166-167**, 581 (2000).
[16] F. Ohnesorge and R. Neumann, Europhys. Lett. **50**, 742 (2000).
[17] K. Nordlund, J. Keinonen, Mai Ghaly, and R. Averback, Nature (London) **398**, 49 (1999).
[18] Z. Insepov and I. Yamada, Nucl. Instrum. Methods Phys. Res. B **148**, 121 (1999).
[19] R. Averback and T. Diaz de la Rubia, in *Solid State Physics*, edited by H. Ehrenreich and F. Spaepen (Academic, New York, 1998), Vol. 51, pp. 281–402.
[20] H. H. Andersen, A. Brunelle, S. Della-Negra, J. Depauw, D. Jacquet, Y. Le Beyec, J. Chaumont, and H. Bernas, Phys. Rev. Lett. **80**, 5433 (1998).
[21] H. H. Andersen, A. Johansen, and V. S. Touboltsev, Nucl. Instrum. Methods Phys. Res. B **163-164**, 727 (2000).
[22] I. Yamada, J. Matsuo, N. Toyoda, T. Aoki, E. Jones, and Z. Insepov, Mater. Sci. Eng., A **253**, 249 (1998).
[23] V. I. Shulga and P. Sigmund, Nucl. Instrum. Methods Phys. Res. B **47**, 236 (1990).
[24] M. Ghaly and R. S. Averback, in *Beam-Solid Interactions: Fundamentals and Applications*, edited by M. A. Nastasi, L. R. Harriott, N. Herhoti, and R. S. Auerbak, Mater. Res. Soc. Symp. Proc. No. 279 (Materials Research Society, Pittsburgh, 1993), p. 17.
[25] Z. Insepov and I. Yamada, Nucl. Instrum. Methods Phys. Res. B **112**, 16 (1996).
[26] T. Aoki, J. Matsuo, Z. Insepov, and I. Yamada, Nucl. Instrum. Methods Phys. Res. B **121**, 49 (1997).
[27] D. Fenyö and R. E. Johnson, Phys. Rev. B **46**, 5090 (1992).
[28] D. E. Gault, J. E. Guest, J. B. Murray, D. Dzurisin, and M. C. Malin, J. Geophys. Res. **80**, 2444 (1975).
[29] A. P. Quist, Å. Petersson, C. T. Reimann, A. A. Bergman, D. D. N. Barlo Daya, A. Hallin, J. Carlsson, S. O. Oscarsson, and B. U. R. Sundqvist, J. Colloid Interface Sci. **189**, 184 (1997).
[30] E. M. Bringa and R. Johnson, Nucl. Instrum. Methods Phys. Res. B **143**, 513 (1998).
[31] E. M. Bringa, R. Johnson, and Ł. Dutkiewicz, Nucl. Instrum. Methods Phys. Res. B **152**, 267 (1999).
[32] E. M. Bringa and R. Johnson, Nucl. Instrum. Methods Phys. Res. B **180**, 99 (2001).
[33] E. M. Bringa, R. E. Johnson, and M. Jakas, Phys. Rev. B **60**, 15 107 (1999).
[34] K. Binder, *Monte Carlo and Molecular Dynamics Simulations in Polymer Science* (Oxford University Press, New York, 1995).
[35] The bulk modulus, which is known from experiments, can be taken proportional to the sublimation energy.
[36] D. W. Van Krevelen, *Properties of Polymers—Their Estimation and Correlation With Chemical Structure* (Elsevier, Amsterdam, 1976).
[37] G. Szenes, K. Havancsák, V. Skuratov, P. Hanak, L. Zsoldos, and

T. Ungár, Nucl. Instrum. Methods Phys. Res. B **166-167**, 933 (2000).
[38] G. Szenes, Phys. Rev. B **52**, 6154 (1995).
[39] E. M. Bringa and R. E. Johnson, Surf. Sci. **451**, 108 (2000).
[40] H. G. Paretzke, D. T. Goodhead, I. G. Kaplan, and M. Terrisol, *Atomic and Molecular Data for Radiotherapy and Radiation Research* (IAEA, Vienna, 1995), pp. 633–739.
[41] R. E. Johnson and J. Schou, Mat. Fys. Medd. K. Dan. Vidensk. Selsk. **43**, 403 (1993).
[42] J. L. Magee and A. Chatterjee, in *Kinetics of Nonhomogeneous Processes*, edited by G. R. Freeman (Wiley, New York, 1987).
[43] M. M. Jakas and E. M. Bringa, Phys. Rev. B **62**, 824 (2000).
[44] Figures of several craters, including 3D views, can be found at http://dirac.ms.virginia.edu/~emb3t/craters/craters.html
[45] Y. Kitazoe, N. Hiraoka, and Y. Yamamura, Surf. Sci. **111**, 381 (1981).
[46] Y. Yamamura, Nucl. Instrum. Methods Phys. Res. **194**, 515 (1982).
[47] M. Jakas, Radiat. Eff. Defects Solids **152**, 157 (2000).
[48] Z. Insepov, R. Manory, J. Matsuo, and I. Yamada, Phys. Rev. B **61**, 8744 (2000).
[49] E. M. Bringa, K. Nordlund, and J. Keinonen, Phys. Rev. B **64**, 235426 (2001).
[50] M. Shapiro and T. Tombrello, Nucl. Instrum. Methods Phys. Res. B **84**, 453 (1994).
[51] B. L. Holian, in *Microscopic Simulations of Complex Hydrodynamic Phenomena*, edited by M. Mareschal and B. L. Holian (Plenum, New York, 1991), pp. 75–86.
[52] M. Moseler, J. Nordiek, and H. Haberland, Phys. Rev. B **56**, 15 439 (1997).
[53] Ya. B. Zel'dovich and Yu. P. Raiser, *Physics of Shock Waves and High Temperature Hydrodynamic Phenomena* (Academic, New York, 1967).
[54] I. S. Bitensky and E. S. Parillis, Nucl. Instrum. Methods Phys. Res. B **21**, 26 (1987).
[55] I. S. Bitensky, A. M. Goldenburg, and E. S. Parilis, in *Ion Formation from Organic Solids V (IFOS V)*, edited by A. Hedin, B. U. R. Sundqvist, and A. Benninghoven (Wiley, Chichester, 1990), p. 205.